SPHERICAL HARMONICS COLLOCATION: A COMPUTATIONAL INTERCOMPARISON OF SEVERAL GRIDS

JEAN-BAPTISTE BELLET[†], MATTHIEU BRACHET[†], AND JEAN-PIERRE CROISILLE[‡]

Abstract. Spherical discrete models are of primary importance in many domains in Computational Physics. In Grid Methods, a particular spherical grid is used in conjunction with a functional approximation procedure, such as finite elements, finite volumes, or collocation. In the traditional pseudospectral approach, a Spherical Harmonics subset is associated to the Longitude-Latitude grid. Here we numerically compare how Spherical Harmonics match three standard grids, the Lon/Lat grid, the equiangular Cubed Sphere and the Icosahedral grid. Our analysis is based on a numerical algorithm providing a specific echelon form of the associated Vandermonde matrix of the couple (Spherical Harmonics subset) / (grid), already introduced in previous works. Numerical results are presented, first in the context of interpolation, and second in the one of quadrature rules. These results support that the Icosahedral grid and of the Cubed Sphere behave better than the traditional Lon/Lat grid. The conclusion is that our interpolation approach is effective on the Icosahedral grid and the Cubed-Sphere. However, it shows deficiencies on the Lon/Lat grid.

1. Introduction

In previous studies, numerical properties of the Cubed Sphere $\mathcal{CS}_N$ as support of collocation of Spherical Harmonics (hereafter called SH functions) have been reported. The associated Vandermonde matrix encodes the basic properties of the collocation procedure of the couple $\mathcal{CS}_N$-nodes/SH functions. From the onset, a suitable SH functions subspace of $\mathcal{Y}_D$ (the SH functions of maximum degree D) canonically associated to $\mathcal{CS}_N$ is not a priori known. In [6], a numerical approach to define such a subspace has been suggested. It is based on a numerical algorithm performing an incremental block echelon factorization of a Vandermonde matrix. A particular SH subspace $\mathcal{U}_D$ emerges from this factorization, where D represents some "cut-off" degree of SH functions supported by the $\mathcal{CS}_N$ grid. Using this SH subspace $\mathcal{U}_D$ on the grid $\mathcal{CS}_N$ makes possible a discrete harmonic calculus. This calculus has been used to perform numerical tasks such as interpolation, approximation, PDE's resolution and numerical quadrature.

Here, we continue this line of analysis by using our echelon algorithm for intercomparing collocation properties of three spherical grids, the Lon/Lat grid, the Cubed Sphere and the Icosahedral grid. These three grids are commonly used in climate simulation on the rotating earth.

The outline is as follows. Section 2 sets the notation. Section 3 presents the numerical algorithm along the lines in [4]. In Section 4 we report elements of numerical intercomparison between the three grids above. This covers in particular the definition of the subspace $\mathcal{U}_D$, condition numbers and interpolation properties. Another outcome, already studied in the case of $\mathcal{CS}_N$ in [5], is the accuracy of spherical quadrature rules associated to the discrete model. The summary in Section 5 mentions some prospects.

2. Notation

The unit sphere $\mathbb{S}^2$ is parametrized by

$$x(\theta,\phi) = (\cos\theta\cos\phi, \cos\theta\sin\phi, \sin\theta) \in \mathbb{S}^2, \quad \theta \in [-\tfrac{\pi}{2}, \tfrac{\pi}{2}], \quad \phi \in \mathbb{R}, \tag{1}$$

with θ, ϕ the latitude/longitude angles. The SH functions of degree $n \geq 0$ is the vector space generated by the functions Y_n^m,

$$Y_n^m(x(\theta,\phi)) = \sqrt{\tfrac{(n+1/2)(n-|m|)!}{\pi(n+|m|)!}} P_n^{(|m|)}(\sin\theta) \cdot \cos^{|m|}\theta \cdot \begin{cases} -\sin m\phi, & -n \leq m < 0, \\ \frac{1}{\sqrt{2}}, & m = 0, \\ \cos m\phi, & 0 < m \leq n, \end{cases} \tag{2}$$

Date: January 14, 2025.

2010 *Mathematics Subject Classification.* 65D05, 65D15, 65D30, 65D32.

Key words and phrases. Spherical grid, interpolation, spherical harmonics, quadrature.

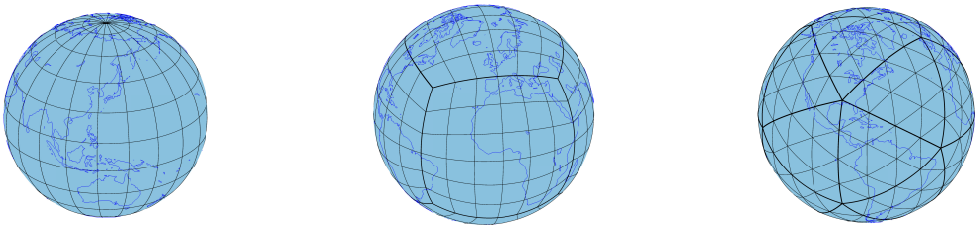

FIGURE 1. Three commonly used spherical grid. The resolution parameter N is ajusted in each case to have a similar resolution. Left: the grid Lon/Lat $\mathcal{LL}_{10}$ with $\bar{N} = 180$ nodes. Center: the Cubed Sphere $\mathcal{CS}_6$ with $\bar{N} = 218$ nodes. Right: the Icosahedral grid $\mathcal{IS}_4$ with $\bar{N} = 162$ nodes.

where $P_n^{(|m|)}(t) = \frac{\mathrm{d}^{|m|}}{\mathrm{d}t^{|m|}} P_n(t)$ is the $|m|$-th derivative of the Legendre polynomial of degree n,

$$P_n(t) = \tfrac{1}{2^n n!} \tfrac{\mathrm{d}^n}{\mathrm{d}t^n}(t^2-1)^n. \tag{3}$$

The family $(Y_n^m)_{|m|\le n,\, n\in\mathbb{N}}$ is a Hilbert basis of the space $L^2(\mathbb{S}^2)$, equipped with the usual inner product and associated norm. The SH subspace of degree n is $\mathbb{Y}_n = \mathrm{span}\{Y_n^m,\, |m| \le n\}$. It consists of the restriction to $\mathbb{S}^2$ of the homogeneous harmonic polynomials of degree n (in $\mathbb{R}^3$). For all degree $M \ge 0$, we denote

$$\mathcal{Y}_M = \mathbb{Y}_0 \oplus \cdots \oplus \mathbb{Y}_M = \mathrm{span}\{Y_n^m,\, |m| \le n,\, 0 \le n \le M\} \tag{4}$$

the space of the SH functions with degree less than or equal to M. Refer to [2, 7].

2.1. **Grid definition.** In the sequel, we will consider the three grids Lon/Lat, Cubed Sphere and Icosahedral. However, our approach is a priori grid independent and can be applied to any set $\mathcal{G}_{\bar{N}} = \{x_i,\, 1 \le i \le \bar{N}\}$ of $\bar{N}$ nodes on $\mathbb{S}^2$. The space of real grid functions defined on $\mathcal{G}_{\bar{N}}$ is $\mathbb{R}^{\mathcal{G}_{\bar{N}}} = \{f : \mathcal{G}_{\bar{N}} \to \mathbb{R}\}$.

The three grids we consider are called $\mathcal{LL}_N$ (longitude-latitude grid), $\mathcal{CS}_N$ (Cubed sphere grid) and $\mathcal{IS}_N$ (Icosahedral grid). They all depend on a resolution parameter $N \in \mathbb{N}$. Fig. 1 shows examples of each grid.

- *Longitude/Latitude grid - $\mathcal{LL}_N$ -* We use the notation in [2]. The grid $\mathcal{LL}_N$ is the set of $\bar{N}_{\mathcal{LL}_N} = 2N^2$ nodes with coordinates

$$\mathcal{LL}_N \triangleq \left\{ \left(\sqrt{1-z_i^2}\cos\tfrac{\pi j}{N}, \sqrt{1-z_i^2}\sin\tfrac{\pi j}{N}, z_i \right),\ 1 \le i \le N \text{ and } 1 \le j \le 2N \right\},$$

  where $z_i \in [-1, 1]$ are the roots of the Legendre polynomial (3) of degree N.
- *Cubed-sphere - $\mathcal{CS}_N$ -* The equiangular Cubed-Sphere is the set $\bar{N}_{\mathcal{CS}_N} = 6N^2 + 2$ nodes defined by

$$\mathcal{CS}_N \triangleq \Big\{ \tfrac{1}{\sqrt{1+u^2+v^2}}(\pm 1, u, v),\ \tfrac{1}{\sqrt{1+u^2+v^2}}(u, \pm 1, v),\ \tfrac{1}{\sqrt{1+u^2+v^2}}(u, v, \pm 1); \\ u = \tan\tfrac{i\pi}{2N}, v = \tan\tfrac{j\pi}{2N}, -\tfrac{N}{2} \le i, j \le \tfrac{N}{2} \Big\}.$$

  The nodes are symmetrically located in 6 panels mirroring the 6 faces of a cube [10].
- *Icosahedral sphere - $\mathcal{IS}_N$ -*
  The icosahedral grid [11] $\mathcal{IS}_N$ is based on 12 nodes evenly distributed over the unit sphere:

$$\left\{ \tfrac{1}{\sqrt{1+\varphi^2}}(\pm\varphi, \pm 1, 0),\ \tfrac{1}{\sqrt{1+\varphi^2}}(\pm 1, 0, \pm\varphi),\ \tfrac{1}{\sqrt{1+\varphi^2}}(0, \pm\varphi, \pm 1) \right\} \quad \text{with } \varphi = \frac{1+\sqrt{5}}{2}.$$

  These 12 nodes define 20 spherical triangles and 30 edges. Each triangle is then tiled with N^2 smaller triangles by inserting $N-1$ uniformly spaced nodes along each edge. Then, the nodes are projected onto the sphere. This construction is referred to as a non recursive approach (see [11,12]). The nodes in $\mathcal{IS}_N$ are obtained by collecting the 12 initial icosahedron vertices, the $30 \times (N-1)$ nodes along each edge and the $20 \times \frac{(N-1)(N-2)}{2}$ nodes in the 20 triangles. This gives $\bar{N}_{\mathcal{IS}_N} = 10N^2 + 2$.

3. Vandermonde matrix

Suppose given a spherical grid $\mathcal{G}_{\bar{N}} = \{x_i,\, 1 \le i \le \bar{N}\}$ and let $(y_j)_{1\le j\le \bar{N}} \in \mathbb{R}^{\mathcal{G}_{\bar{N}}}$ be a grid function. We wish to find $p \in \mathcal{Y}_D$ a SH function interpolating y, i.e.

$$p(x_j) = y_j \qquad 1 \le j \le \bar{N}. \tag{5}$$

We need to determine a degree $D \in \mathbb{N}$ and a suitable subspace $\mathcal{U}_D \subset \mathcal{Y}_D$, such that problem (5) has an unique solution. For this purpose, consider the sequence of Vandermonde matrices associated to the grid $\mathcal{G}_{\bar{N}}$ defined by

Definition 1 (sequence of Vandermonde matrices of $\mathcal{G}_{\bar{N}}$)**.** For any $n \ge 0$, we call $\mathbf{A}_n$ the Vandermonde matrix

$$\mathbf{A}_n \triangleq [Y_k^m(x_j)]_{1\le j\le \bar{N},\, |m|\le k\le n} \in \mathbb{R}^{\bar{N}\times(n+1)^2}, \tag{6}$$

with line index, the nodes in $\mathcal{G}_{\bar{N}}$ and column index, the couples (k,m) sorted in lexicographical order.

The matrix $\mathbf{A}_n$, has a block structure, where each block $\mathbf{A}_k$ corresponds to the SH functions $(Y_k^m)_{|m|\le k}$ restricted to $\mathcal{G}_{\bar{N}}$

$$\mathbf{A}_n = \begin{bmatrix} A_0 & A_1 & \cdots & A_n \end{bmatrix} \in \mathbb{R}^{\bar{N}\times(n+1)^2}, \quad \text{with} \quad A_k \triangleq [Y_k^m(x_j)]_{1\le j\le \bar{N},\, |m|\le k} \in \mathbb{R}^{\bar{N}\times(2k+1)}. \tag{7}$$

Once the integer D is given, calculating the polynomial p in (5) proceeds as follows:

- determine a vector $[\hat{p}_n^m]_{|m|\le n\le D} \in \mathbb{R}^{(D+1)^2}$ such that
$$\mathbf{A}_D[\hat{p}_n^m]_{|m|\le n\le D} = [y_j]_{1\le j\le \bar{N}}, \tag{8}$$
- evaluate the polynomial $p(x) \triangleq \displaystyle\sum_{|m|\le n\le D} \hat{p}_n^m Y_n^m(x)$ in matrix-vector form by
$$p(x) = [Y_n^m(x)]^{\intercal}_{|m|\le n\le D}[\hat{p}_n^m]_{|m|\le n\le D}. \tag{9}$$

3.1. Theoretical approach to the SH subspace $\mathcal{U}_D$.

Here we define a subspace of SH functions $\mathcal{U}_D$ ensuring existence and uniqueness in (5). We begin with the following lemma which is a direct consequence of [8, Lemma 3.13]. It states that the interpolation problem (5) has at least a solution provided that the integer D is selected large enough.

Lemma 2. *Define the separation distance* $\operatorname{sep}(\mathcal{G}_{\bar{N}}) = \min_{i\ne j} \arccos(x_j^{\intercal} x_i)$*, the minimal distance between two distinct nodes of* $\mathcal{G}_{\bar{N}}$*. Let* $q > 0$ *and* $D \in \mathbb{N}$ *satisfying*

$$0 < q < \operatorname{sep}(\mathcal{G}_{\bar{N}}), \quad D \ge \frac{7.5\pi}{q}.$$

Then the matrix $\mathbf{A}_D$ *has a full row rank. In other words, any grid function* $f \in \mathbb{R}^{\mathcal{G}_{\bar{N}}}$ *can be interpolated by at least one SH function* $u \in \mathcal{Y}_D$*.*

Existence in problem (5) is thus guaranteed for all $D > \left\lfloor \dfrac{7.5\pi}{q} \right\rfloor$. Next, we proceed by induction on the degree n to define a SH functions set ensuring in addition uniqueness in (5) [4–6]. This is summarized in the following theorem.

Theorem 3 (Interpolation space)**.** *Consider the subspace* W_n *of the SH functions of degree* n*, inductively defined by*

$$\mathcal{W}_0 \triangleq \{0\}, \quad \mathcal{W}_n \triangleq \{w \in \mathbb{Y}_n : \exists v \in \mathbb{Y}_0 \oplus \cdots \oplus \mathbb{Y}_{n-1}, w|_{\mathcal{G}_{\bar{N}}} = v|_{\mathcal{G}_{\bar{N}}}\}, n \ge 1, \tag{10}$$

and consider the decomposition

$$\mathbb{Y}_n = \mathcal{W}_n \overset{\perp}{\oplus} \mathcal{W}_n^{\perp}, \quad n \ge 0. \tag{11}$$

Let T *denote the restriction operator on* $\mathcal{G}_{\bar{N}}$*,*

$$\begin{array}{rccc} T: & \mathscr{C}^0(\mathbb{S}^2) & \longrightarrow & \mathbb{R}^{\mathcal{G}_{\bar{N}}} \\ & u & \longmapsto & T(u) \triangleq u|_{\mathcal{G}_{\bar{N}}} \end{array}. \tag{12}$$

Then there exists a smallest degree $D = D(\mathcal{G}_{\bar{N}}) \ge 0$ *such that the linear map* $T_D \triangleq T|_{\mathcal{W}_0^{\perp}\oplus\cdots\oplus\mathcal{W}_D^{\perp}}$ *is isomorphic. The interpolation space is then defined as*

$$\mathcal{U}_D \triangleq \mathcal{W}_0^{\perp} \oplus \cdots \oplus \mathcal{W}_D^{\perp}. \tag{13}$$

The inverse of T_D *is called the interpolation operator and is denoted by* $\mathcal{I}_{\bar{N}} : \mathbb{R}^{\mathcal{G}_{\bar{N}}} \to \mathcal{U}_D$*.*

Proof. First, we prove by induction on the degree $n \geq 0$, that

$$T(\mathbb{Y}_0 \oplus \cdots \oplus \mathbb{Y}_n) = T(\mathcal{W}_0^\perp \oplus \cdots \oplus \mathcal{W}_n^\perp). \tag{14}$$

For $n = 0$, this is due to $\mathbb{Y}_0 = \mathcal{W}_0^\perp$. Fix now $n \geq 1$ such that (14) holds for the degree $n-1$ (induction). By definition of $\mathcal{W}_n$, $\mathbb{Y}_n = \mathcal{W}_n \oplus \mathcal{W}_n^\perp$, with $T(\mathcal{W}_n) \subset T(\mathbb{Y}_0 \oplus \cdots \oplus \mathbb{Y}_{n-1})$. Therefore

$$T(\mathbb{Y}_0 \oplus \cdots \oplus \mathbb{Y}_n) = T(\mathbb{Y}_0 \oplus \cdots \oplus \mathbb{Y}_{n-1} \oplus \mathcal{W}_n^\perp) = T(\mathcal{W}_0^\perp \oplus \cdots \oplus \mathcal{W}_n^\perp),$$

which achieves the induction.

Second, fix $D = \left\lfloor \dfrac{7.5\pi}{q} \right\rfloor + 1$ where $\mathrm{sep}(\mathcal{G}_{\bar{N}}) > q > 0$. Lemma 2 shows that the linear map $T|_{\mathbb{Y}_0 \oplus \cdots \oplus \mathbb{Y}_D}$ is surjective; hence, (14) with $n = D$ implies that the restriction T_D is surjective as well.

To conclude, we prove that T_D is also injective. Assume that there is $w \in \mathcal{W}_0^\perp \oplus \cdots \oplus \mathcal{W}_D^\perp \setminus \{0\}$ such that $Tw = 0$. Let $n \leq D$ be the degree of w. The unique constant function $u \in \mathbb{Y}_0$ such that $u|_{\mathcal{G}_{\bar{N}}} = 0$ is the zero function, therefore $n \geq 1$. Then, there exist $w_n \in \mathcal{W}_n^\perp \setminus \{0\}$ and $y \in \mathbb{Y}_0 \oplus \cdots \oplus \mathbb{Y}_{n-1}$ such that $w = w_n - y$. Since $Tu = 0$, $w_n|_{\mathcal{G}_{\bar{N}}} = y|_{\mathcal{G}_{\bar{N}}}$, so $w_n \in \mathcal{W}_n$, which is a contradiction. □

The subspace $\mathcal{W}_n$ represents the SH functions of degree n which are undersampled on $\mathcal{G}_{\bar{N}}$. This means that they coincide on $\mathcal{CS}_N$ with a SH function of smaller degree. On the other hand, all the SH functions in $\mathcal{W}_n^\perp$ are properly sampled on $\mathcal{G}_{\bar{N}}$, since they can be reconstructed by interpolation. Consequently, the SH subspace $\mathcal{U}_D$ is intrinsically defined by (13). At this stage, there is no analytical description of $\mathcal{U}_D$, nor of $\mathcal{W}_n$, $\mathcal{W}_n^\perp$: their definitions are purely theoretical.

By construction of the space $\mathcal{U}_D$ in (13) and of the interpolation operator $\mathcal{I}_{\bar{N}}$ in (12), the Lagrange interpolation problem on $\mathcal{G}_{\bar{N}}$ has a unique solution in $\mathcal{U}_D$. Furthermore, for every $f \in \mathbb{R}^{\mathcal{G}_{\bar{N}}}$, $\mathcal{I}_{\bar{N}} f \in \mathcal{U}_D$ denotes the unique element $p \in \mathcal{U}_D$ such that $p|_{\mathcal{G}_{\bar{N}}} = f$. The following result states that the degree of $\mathcal{I}_{\bar{N}} f$ is actually minimal.

Corollary 4 (Minimal degree)**.** *Let $f \in \mathbb{R}^{\mathcal{G}_{\bar{N}}}$ be a grid function interpolated by $\mathcal{I}_{\bar{N}} f \in \mathcal{U}_D$. Let $u \in \mathbb{Y}_0 \oplus \cdots \oplus \mathbb{Y}_{\tilde{D}}$ be a SH function of degree $\tilde{D}$ interpolating f,* i.e. *$u|_{\mathcal{G}_{\bar{N}}} = f$. Then $\tilde{D} \geq \deg(I_{\bar{N}} f)$.*

Proof. If $\tilde{D} > D$, the result is obvious. If $\tilde{D} \leq D$, $f = Tu \in T(\mathbb{Y}_0 \oplus \cdots \oplus \mathbb{Y}_{\tilde{D}})$. By (14) there exists a $v \in \mathcal{W}_0^\perp \oplus \cdots \oplus \mathcal{W}_{\tilde{D}}^\perp$ such that $f = Tv$ with $\tilde{D} \leq D$. Hence, $v \in \mathcal{U}_D$, which implies $v = \mathcal{I}_{\bar{N}} f$. Therefore,

$$\deg(\mathcal{I}_{\bar{N}} f) = \deg(v) \leq \tilde{D}. \tag{15}$$

□

Remark 5. The approximation power of $\mathcal{U}_D$ is estimated by the distance $dist(Y_n^m, \mathcal{U}_D)$ of a given SH function Y_n^m to $\mathcal{U}_D$. It turns out that on the one hand, for $n > D$, we have $\mathbb{Y}_n \perp \mathcal{U}_D$ so that $dist(Y_n^m, \mathcal{U}_D) = 1$. On the other hand, for n small enough, $\mathcal{Y}_n \subset \mathcal{U}_D$, so that $dist(Y_n^m, \mathcal{U}_D) = 0$. In this case, Y_n^m is exactly recovered by interpolation in $\mathcal{U}_D$. In Section 4, the distance $dist(Y_n^m, \mathcal{U}_D)$ with $|m| \leq n \leq D$ is numerically evaluated.

3.2. **Echelon factorization algorithm.** In [6], a factorization of the Vandermonde matrix (7) has been introduced in the case of the Cubed Sphere $\mathcal{CS}_N$. This factorization is obtained as the final stage of an incremental algorithm of special echelon kind. Here we show that this algorithm can be used in the case of a general grid.

Theorem 6 (Special echelon orthogonal factorization [4, 6])**.** *Let $\mathcal{G}_{\bar{N}}$ be a spherical grid and $n \geq 0$. The Vandermonde matrix $\mathbf{A}_n \in \mathbb{R}^{\bar{N} \times (n+1)^2}$ in* (7) *can be factorized in special echelon form as*

$$\mathbf{A}_n = \mathbf{V}_n \mathbf{E}_n \mathbf{U}_n^\intercal, \tag{16}$$

where

- *the matrix $\mathbf{V}_n \in \mathbb{R}^{\bar{N} \times \bar{N}}$ is orthogonal,*
- *the matrix $\mathbf{U}_n = \begin{bmatrix} U_0 & 0 & \cdots & 0 \\ 0 & U_1 & \ddots & \vdots \\ \vdots & \ddots & \ddots & 0 \\ 0 & \cdots & 0 & U_n \end{bmatrix}$ is block diagonal and for $1 \leq k \leq n$, $U_k \in \mathbb{R}^{(2k+1)\times(2k+1)}$ is orthogonal,*

- *the matrix* $\mathbf{E}_n = \begin{bmatrix} \Lambda_0 & * & \cdots & * \\ 0 & \Lambda_1 & \ddots & \vdots \\ \vdots & \ddots & \ddots & * \\ 0 & \cdots & 0 & \Lambda_n \\ 0 & \cdots & \cdots & 0 \end{bmatrix} \in \mathbb{R}^{\bar{N}\times(n+1)^2}$ *is in echelon form, with* Λ_k *the block matrix*

$$\Lambda_k = \left[\begin{array}{cccc|c} d_1^k & 0 & \cdots & 0 & \\ 0 & d_2^k & \ddots & \vdots & \\ \vdots & \ddots & \ddots & 0 & \mathbf{0}_{g_k,2k+1-g_k} \\ 0 & \cdots & 0 & d_{g_k}^k & \end{array}\right] \tag{17}$$

for some $g_k \geq 0$ *and with* $d_1^k \geq d_2^k \cdots \geq d_{g_k}^k > 0$.

The proof is similar to the one in [6, Theorem 7] and it is not reproduced here. It proceeds by induction on the degree n. The factorization (16) is the matrix representation of the decomposition (11). The matrix $\mathbf{U}_n$ encodes orthonormal bases of the spaces $\mathcal{W}_k^\perp$ and $\mathcal{W}_k$, $0 \leq k \leq n$ as described in the following definition.

Definition 7 (Basis functions of the SH function spaces $\mathcal{W}_k$ and $\mathcal{W}_k^\perp$ in (11))**.** Let $n \geq 0$, and consider the special echelon form (16) of $\mathbf{A}_n$. Then

- For all $0 \leq k \leq n$ and $1 \leq i \leq 2k+1$, the set of functions $u_k^i(x) \in \mathbb{Y}_k$ defined by
$$u_k^i \in \mathbb{Y}_k, \quad u_k^i(x) = [Y_k^m(x)]_{|m|\leq k}^\intercal U_k(:,i),\ x \in \mathbb{S}^2, \tag{18}$$
forms a basis of $\mathbb{Y}_k$.
- the set $\{u_k^i,\ 1 \leq i \leq g_k\}$ forms an orthonormal basis of the space $\mathcal{W}_k^\perp$.
- the set $\{u_k^i,\ g_k+1 \leq i \leq 2k+1\}$ forms an orthonormal basis of the undersampled space $\mathcal{W}_k$.

Next, consider the submatrix $\tilde{\mathbf{U}}_n$ of $\mathbf{U}_n$

$$\tilde{\mathbf{U}}_n = \begin{bmatrix} U_0(1:1,1:g_0) & & \\ & \ddots & \\ & & U_n(1:2n+1,1:g_n) \end{bmatrix} \in \mathbb{R}^{(n+1)^2\times \mathrm{rank}(\mathbf{A}_n)}. \tag{19}$$

The matrix $\mathbf{A}_n\tilde{\mathbf{U}}_n$ represents the operator $T|_{\mathcal{W}_0^\perp\oplus\cdots\oplus\mathcal{W}_n^\perp}$ in the basis $\{u_k^i,\ 1 \leq i \leq g_k,\ 0 \leq k \leq n\}$ with full column rank $r_n = g_0 + \cdots + g_n$. It has the QR factorization

$$\mathbf{A}_n\tilde{\mathbf{U}}_n = \mathbf{V}_n\tilde{\mathbf{E}}_n, \tag{20}$$

where $\tilde{\mathbf{E}}_n$ is an upper triangular matrix with full column rank deduced from $\mathbf{E}_n$. The QR factorization (20) with $n = D$ is

$$\mathbf{A}_D\tilde{\mathbf{U}}_D = \mathbf{V}_D\tilde{\mathbf{E}}_D. \tag{21}$$

The relation (21) provides an orthonormal basis $\{u_k^i,\ 1 \leq i \leq g_k,\ 0 \leq k \leq D\}$ of the space $\mathcal{U}_D$, and a QR form of the operator $T_D : \mathcal{U}_D \to \mathbb{R}^{\mathcal{G}_{\bar{N}}}$, where $\mathbf{V}_D$ is orthogonal, and the upper triangular matrix $\tilde{\mathbf{E}}_D \in \mathbb{R}^{\bar{N}\times\bar{N}}$ is non-singular. It results from Theorem 3 that $\mathbf{A}_D\tilde{\mathbf{U}}_D$ is non-singular, and that the row rank of $\mathbf{A}_n\tilde{\mathbf{U}}_n$ is deficient if $n < D$ (i.e. $r_n < \bar{N}$). This suggests to compute incrementally the factorization (16), for increasing values of n, until the value of $r_n = g_0 + \cdots + g_n$ reaches the size of the grid $\bar{N}$. This is implemented in the Algorithm 1. The numerical resolution of the problem (5) is given by

Corollary 8 (solution of the interpolation problem (5))**.** *Assume that the factorization* (21) *has been precomputed. Let* $f \in \mathbb{R}^{\mathcal{G}_{\bar{N}}}$ *be a grid function. Then, the unique element* $u \in \mathcal{U}_D$ *such that* $u(x_j) = f(x_j)$, $1 \leq j \leq \bar{N}$, *is given by*

$$\mathcal{I}_{\bar{N}}[f](x) = [Y_n^m(x)]_{|m|\leq n\leq D}^\intercal [\hat{p}_n^m]_{|m|\leq n\leq D}, \quad \textit{with} \quad [\hat{p}_n^m]_{|m|\leq n\leq D} = \tilde{\mathbf{U}}_D(\tilde{\mathbf{E}}_D)^{-1}\mathbf{V}_D^\intercal\,[f(x_j)]_{1\leq j\leq\bar{N}}.$$

The vector $\alpha \triangleq (\tilde{\mathbf{E}}_D)^{-1}\mathbf{V}_D^\intercal\,[f(x_j)]_{1\leq j\leq\bar{N}}$ *is obtained by backward substitution in the upper triangular system*

$$\tilde{\mathbf{E}}_D\,\alpha = \mathbf{V}_D^\intercal\,[f(x_j)]_{1\leq j\leq\bar{N}}.$$

Proof. The matrix of $\mathcal{I}_{\bar{N}} = T_D^{-1}$ is given by $(\mathbf{A}_D\tilde{\mathbf{U}}_D)^{-1} = (\tilde{\mathbf{E}}_D)^{-1}\mathbf{V}_D^\intercal$, due to (21). □

Algorithm 1 Incremental special echelon orthogonal factorization of Vandermonde matrices

Require: Set of $\bar{N}$ nodes on the sphere: $\mathcal{G}_{\bar{N}}$.

Initialization. For $n = 0$, compute the factorization $\mathbf{A}_0 = \mathbf{V}_0\mathbf{E}_0\mathbf{U}_0^\intercal$:

1. compute the matrix $\mathbf{A}_0$ in (7);
2. compute the matrices $\mathbf{V}_0$, $\mathbf{E}_0$ and $\mathbf{U}_0$ by SVD of $\mathbf{A}_0$;
3. evaluate the number of nonzero diagonal coefficients in $\mathbf{E}_0$, $r_0 = g_0$.

Iterations For $n \geq 1$, compute the factorization $\mathbf{A}_n = \mathbf{V}_n\mathbf{E}_n\mathbf{U}_n^\intercal$:

1. compute the matrix A_n in (7);
2. compute matrices V_n, $\begin{bmatrix}\Lambda_n \\ 0\end{bmatrix}$ and U_n by SVD :
$$\mathbf{V}_{n-1}(:, r_{n-1}+1 : \bar{N})^\intercal A_n = V_n \begin{bmatrix}\Lambda_n \\ 0\end{bmatrix} U_n^\intercal.$$
3. assemble the matrices $\mathbf{V}_n$, $\mathbf{E}_n$ and $\mathbf{U}_n$ defined by
$$\mathbf{V}_n = \mathbf{V}_{n-1}\begin{bmatrix}\mathrm{I}_{r_{n-1}} & 0 \\ 0 & V_n\end{bmatrix}$$
$$\mathbf{U}_n = \begin{bmatrix}\mathbf{U}_{n-1} & 0 \\ 0 & U_n\end{bmatrix}$$
$$\mathbf{E}_n = \begin{bmatrix}\mathbf{E}_{n-1}(1 : r_{n-1}, :) & \mathbf{V}_{n-1}(:, 1 : 1 : r_{n-1})^\intercal A_n U_n \\ 0 & \Lambda_n \\ 0 & 0\end{bmatrix};$$
4. evaluate the number g_n of nonzero diagonal coefficients in $\begin{bmatrix}\Lambda_n \\ 0\end{bmatrix}$, and evaluate the rank of $\mathbf{A}_n$ with $r_n = r_{n-1} + g_n$.

Stopping criterion. Exit when $r_n = \bar{N}$.

Output :

- Smallest degree D such that the Vandermonde matrix $\mathbf{A}_D$ in (6) has full row rank
- Associated echelon factorization (16): $\mathbf{A}_D = \mathbf{V}_D\mathbf{E}_D\mathbf{U}_D^\intercal$.

4. Numerical results

4.1. **Echelon factorization accuracy.** In Theorem 3, the integer D has been defined as the maximum degree such that the space $\mathcal{U}_D$ is properly represented by the grid $\mathcal{G}_{\bar{N}}$. The factorization (16) and the QR factorization (21) depend on D (Algorithm 1) and are defined in exact arithmetic. In inexact arithmetic, the dimensions g_n in (17) are evaluated using a thresholding τ on the coefficients of $\Delta_n = \begin{bmatrix}\Lambda_n \\ 0\end{bmatrix}$, with Λ_n the positive diagonal matrix defined in Theorem 6. For a given value of the threshold $\tau > 0$, we let $\Delta_n = 0$ if $[\Delta_n]_{1,1} \leq \tau$; otherwise, for all $i \geq 1$ such that $\frac{[\Delta_n]_{i,i}}{[\Delta_n]_{1,1}} \leq \tau$, we let $[\Delta_n]_{i,i} = 0$. With this convention, the computed factorization is inexact and both the computed degree D and the computed space $\mathcal{U}_D$ depend on the selected threshold τ. For each grid $\mathcal{LL}_N$, $\mathcal{CS}_N$ and $\mathcal{IS}_N$, we investigate how the threshold level τ influences the degree D, the accuracy of the factorization (20) and the condition number of the matrices $\mathbf{A}_D$ and $\tilde{\mathbf{E}}_D$.

4.1.1. *Degree D of the subspace $\mathcal{U}_D$ in* (13). Fig. 2, top line, reports the degree D corresponding to the interpolation space $\mathcal{U}_D$ when picking the threshold $\tau = \tau_1 = 10^{-4}$, $\tau = \tau_2 = 10^{-2}$ and $\tau = \tau_3 = 10^{-1}$, respectively. Note that $\tau' \geq \tau''$ leads to $D(\tau') \geq D(\tau'')$. Fig. 2, bottom line, shows that

- the Lon/Lat grid $\mathcal{LL}_N$ requires SH functions of higher degree D;
- the grids $\mathcal{CS}_N$ and $\mathcal{IS}_N$ require almost identical values of D (slightly lower for $\mathcal{IS}_N$).

For a given grid $\mathcal{G}_{\bar{N}}$ and a fixed n, the larger is the space W_n in (11), the smaller is the space $W_n^\perp$ and therefore the smaller is D. This leads to assert that a lower value of D is associated with a more accurate representation of low-degree SH functions on $\mathcal{G}_{\bar{N}}$. From the 3 top panels in Fig. 2, it results that for a fixed threshold τ, the grids $\mathcal{CS}_N$ and $\mathcal{IS}_N$ provide a better representation of low-degree SH functions than $\mathcal{LL}_N$. In addition, a smaller threshold τ is associated with a larger maximum degree D. Therefore the threshold τ should be picked as not too small.

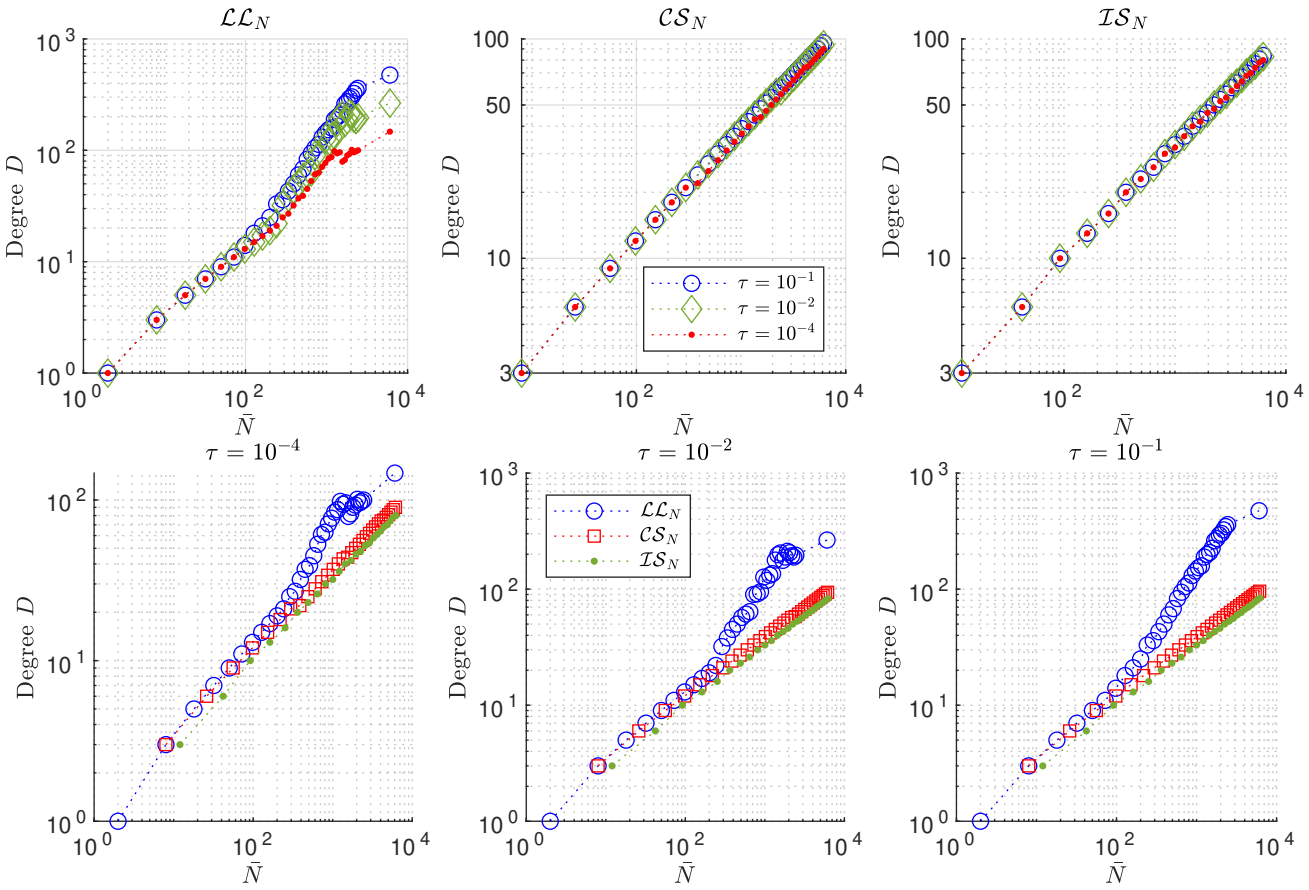

FIGURE 2. Plots of the degree D of the interpolation space $\mathcal{U}_D$ (see (13)) with the three grids $\mathcal{LL}_N$, $\mathcal{CS}_N$ and $\mathcal{IS}_N$ and for the three threshold values $\tau_1 = 10^{-4}$, $\tau_2 = 10^{-2}$ and $\tau_3 = 10^{-1}$. The 3 top panels show $\bar{N} \mapsto D$ for the grid $\mathcal{LL}_N$, $\mathcal{CS}_N$ and $\mathcal{IS}_N$, (left to right), comparing in each plot the 3 threshold values $\tau = \tau_1$, $\tau = \tau_2$ and $\tau = \tau_3$. For each grid, the larger is τ, the larger is D. The 3 bottom panels show $\bar{N} \mapsto D$ for $\tau = \tau_1$, $\tau = \tau_2$ and $\tau = \tau_3$ (left to right), comparing in each plot the 3 grids $\mathcal{LL}_N$, $\mathcal{CS}_N$ and $\mathcal{IS}_N$. This shows $D_{\mathcal{LL}_N} > D_{\mathcal{CS}_N} > D_{\mathcal{IS}_N}$. A smaller D means better approximation properties of the grid.

4.1.2. *Accuracy in the factorization* (20). We comment on the accuracy of the factorisation (20) with the three threshold values $\tau_1 = 10^{-4}$, $\tau_2 = 10^{-2}$ and $\tau_3 = 10^{-4}$, the three grids $\mathcal{LL}_N$, $\mathcal{CS}_N$ and $\mathcal{IS}_N$ and for various grid sizes $\bar{N}$. Fig. 3 reports the relative error

$$\bar{N} \mapsto \frac{\|\mathbf{A}_D\tilde{\mathbf{U}}_D - \mathbf{V}\tilde{\mathbf{E}}_D\|_2}{\|\mathbf{A}_D\tilde{\mathbf{U}}_D\|_2}, \tag{22}$$

(see Theorem 6 and Corollary 8 for the notation). In almost all cases, the error is close to 10^{-14} regardless of the grid and of the threshold level τ. For the grid $\mathcal{CS}_N$ with $\bar{N} \gtrsim 10^3$, (22) reaches the highest obtained error level ($\simeq 10^{-11}$). Overall, Algorithm 1 gives accurate results in the tested cases. Note that the slightly higher error for the finest grids $\mathcal{CS}_N$.

4.1.3. *Condition numbers* $\mathrm{cond}(\mathbf{A}_D)$ *and* $\mathrm{cond}(\tilde{\mathbf{E}}_D)$. The matrix $\mathbf{A}_D$ represents how the grid $\mathcal{G}_{\bar{N}}$ interpolates the full subspace $\mathcal{Y}_D$. Therefore, on the one hand, the condition number $\mathrm{cond}(\mathbf{A}_D)$ gives an indication on the accuracy and stability of the problem (8). On the other hand, the matrix $\mathbf{A}_D\tilde{\mathbf{U}}_D$ corresponds to the interpolation operator in the subspace $\mathcal{U}_D$. Since the matrix $\mathbf{V}_D$ is orthogonal the accuracy of the interpolation operator is related to $\mathrm{cond}(\tilde{\mathbf{E}}_D)$. We report the accuracy numerical in Table 1 and Fig. 4. Table 1 reports the smallest $\bar{N}$ such that $\mathrm{cond}(\mathbf{A}_D) > 10^3$ (for each grid and for τ_1, τ_2 and τ_3). In all cases, one observes that

$$\mathrm{cond}(\mathbf{A}_D)_{\mathcal{IS}_N} < \mathrm{cond}(\mathbf{A}_D)_{\mathcal{CS}_N} < \mathrm{cond}(\mathbf{A}_D)_{\mathcal{LL}_N} \tag{23}$$

Fig. 4 reports $\bar{N} \mapsto \mathrm{cond}(\mathbf{A}_D)$ and $\bar{N} \mapsto \mathrm{cond}(\tilde{\mathbf{E}}_D)$ for the three grids and threshold values $\tau_1 = 10^{-4}$, $\tau_2 = 10^{-2}$ and $\tau_3 = 10^{-1}$. In all cases, we observe that $\mathrm{cond}(\mathbf{A}_D) \leq \mathrm{cond}(\tilde{\mathbf{E}}_D)$. Selecting the space $\mathcal{U}_D$ in $\mathcal{Y}_D$ increases the condition number: it is a price to pay to have an isomorphism in the resolution of (8). In

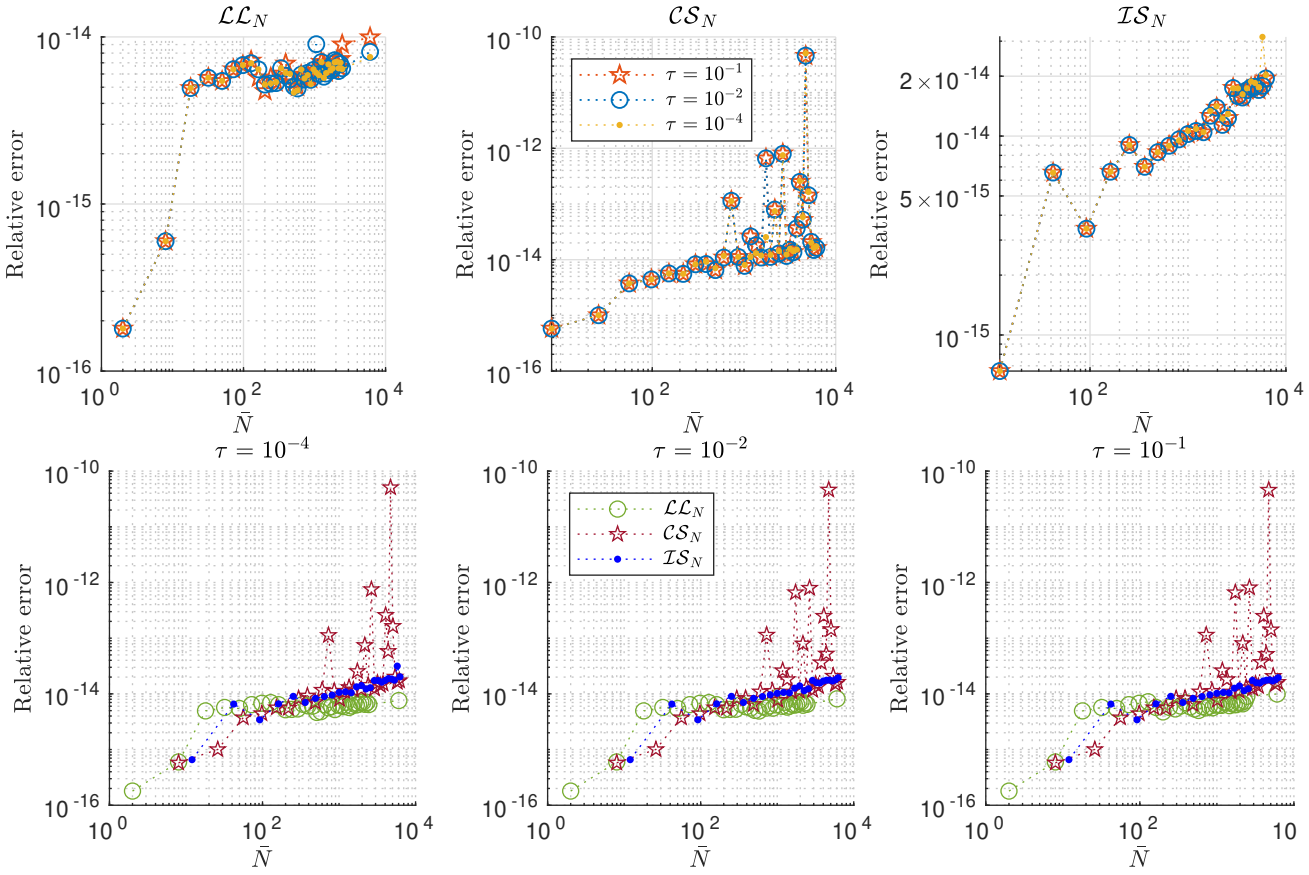

FIGURE 3. Plots of the factorization error (22) with the three grids $\mathcal{LL}_N$, $\mathcal{CS}_N$ and $\mathcal{IS}_N$ and for the three threshold values $\tau = \tau_1 = 10^{-4}$, $\tau = \tau_2 = 10^{-2}$ and $\tau = \tau_3 = 10^{-1}$. The 3 top panels show the function (22). Each color corresponds to a threshold $\tau \in \{\tau_1, \tau_2, \tau_3\}$. The magnitude of the error is about 10^{-14} except for $\mathcal{CS}_N$, where it can reach 10^{-11}. The 3 bottom panels show $\bar{N} \mapsto (22)$ for $\tau = \tau_1$, $\tau = \tau_2$ and $\tau = \tau_3$ (left to right), comparing in each plot the 3 grids $\mathcal{LL}_N$, $\mathcal{CS}_N$ and $\mathcal{IS}_N$.

	$\mathcal{LL}_N$	$\mathcal{CS}_N$	$\mathcal{IS}_N$
$\tau = \tau_1 = 10^{-4}$	128	386	2892
$\tau = \tau_2 = 10^{-2}$	128	> 6000	> 6000
$\tau = \tau_3 = 10^{-1}$	1152	> 6000	> 6000

TABLE 1. Minimal number of nodes $\bar{N}$ for which $\text{cond}(\mathbf{A}_D) > 10^3$ for the grids $\mathcal{LL}_N$, $\mathcal{CS}_N$ and $\mathcal{IS}_N$ and for $\tau \in \{\tau_1, \tau_2, \tau_3\}$. (A large value means accurate results). The number of nodes $\bar{N}$ is the largest for the grid $\mathcal{IS}_N$ and the smallest for the grid $\mathcal{LL}_N$.

addition, the smaller is the threshold τ, the larger is the degree D and the larger is the condition number of the matrices $\mathbf{A}_D$ and $\tilde{\mathbf{E}}_D$. Our experience shows that a threshold value $\tau = \tau_2 = 10^{-2}$ is suitable in most of the cases. This value is adopted in Section 4.3 (interpolation) and 4.4 (quadrature).

4.2. **Subspace $\mathcal{U}_D$.** Consider the expansion of $f \in L^2(\mathbb{S})$ into a series of SH functions. At the discrete level, this expansion translates to the decomposition of $T(f) \in \mathbb{R}^{\mathcal{G}}_{\bar{N}}$ onto the basis $(u_k^i)_{1\le i\le g_k, 0\le k\le D}$. Consider a SH function Y_n^m (with $0 \le |m| \le n$). The ability of the grid $\mathcal{G}_{\bar{N}}$ to sample Y_n^m is measured with the distance $dist(Y_n^m, \mathcal{U}_D) = \inf_{u\in\mathcal{U}_D} \|Y_n^m - u\|_{L^2(\mathbb{S}^2)}$. One has $dist(Y_n^m, \mathcal{U}_D) = 0$ (resp. 1) if $Y_n^m \in \mathcal{U}_D$ (resp. $Y_n^m \perp \mathcal{U}_D$). The matrix $\tilde{\mathbf{U}}_D \tilde{\mathbf{U}}_D^\intercal$ represents the orthogonal projection onto $\mathcal{U}_D$. Therefore, for $0 \le |m| \le n \le D$,

$$\left[dist(Y_n^m, \mathcal{U}_D)\right]_{0\le|m|\le n\le D} = \left[\left\| c_j\left(\mathrm{I} - \tilde{\mathbf{U}}_D \tilde{\mathbf{U}}_D^\intercal\right)\right\|_2\right]_{1\le j\le (D+1)^2} \tag{24}$$

where $c_j(M)$ stands for the j- th column of the matrix M. Displaying the matrix (24) is a convenient way to represent the subspace $\mathcal{U}_D$. An example is given in Fig. 5, which represents (24) for the grids $\mathcal{LL}_{55}$,

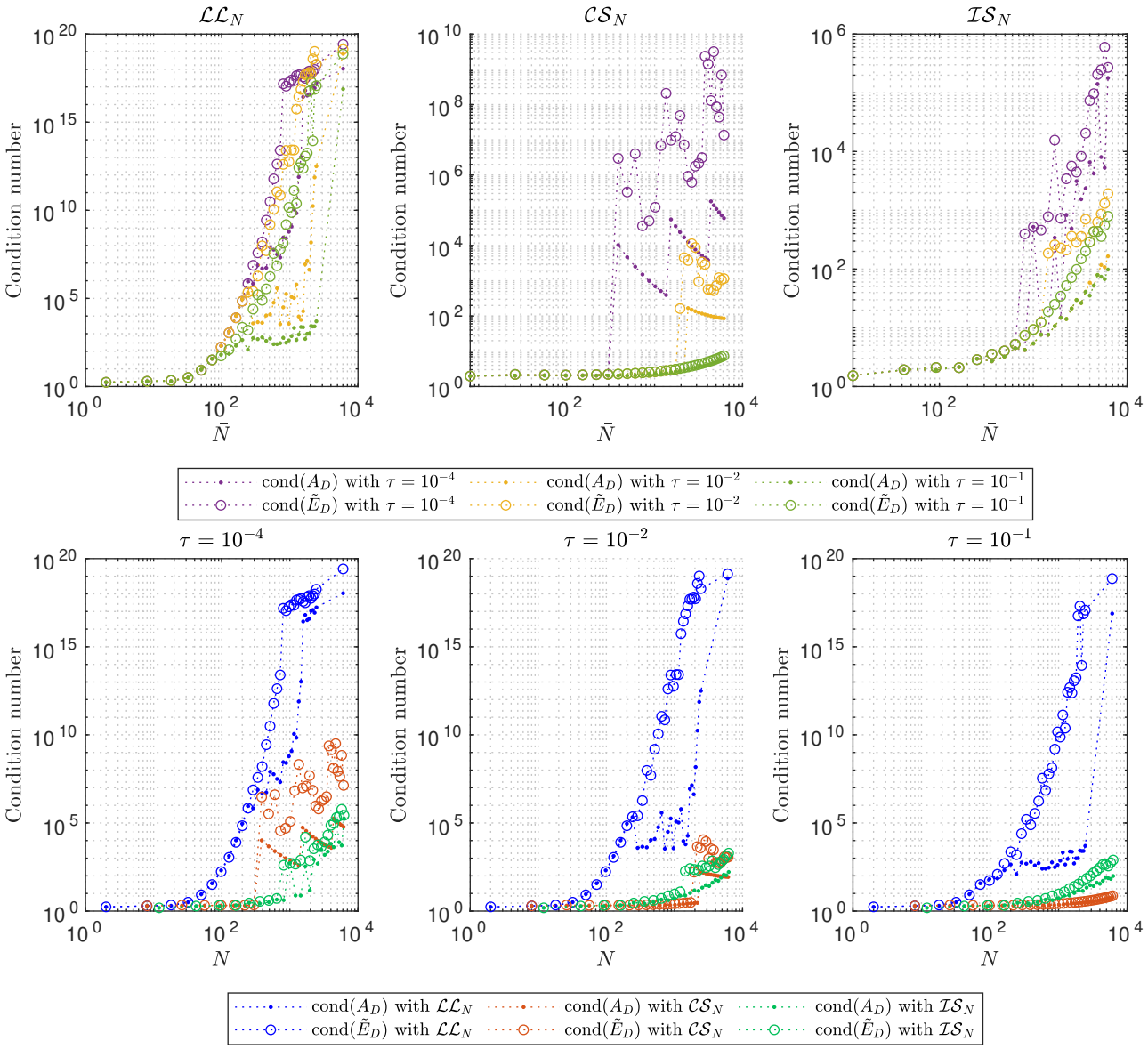

FIGURE 4. Plots of the Condition numbers cond($\mathbf{A}_D$) and cond($\mathbf{E}_D$) with with the three grids $\mathcal{LL}_N$, $\mathcal{CS}_N$ and $\mathcal{IS}_N$ and for the three threshold values $\tau = \tau_1 = 10^{-4}$, $\tau = \tau_2 = 10^{-2}$ and $\tau = \tau_3 = 10^{-1}$. The 3 top panels show $\bar{N} \mapsto \text{cond}(\mathbf{A}_D)$ and $\bar{N} \mapsto \text{cond}(\mathbf{E}_D)$ for the grid $\mathcal{LL}_N$, $\mathcal{CS}_N$ and $\mathcal{IS}_N$, (left to right), comparing in each plot the 3 threshold values $\tau = \tau_1$, $\tau = \tau_2$ and $\tau = \tau_3$. The 3 bottom panels show $\bar{N} \mapsto \text{cond}(\mathbf{A}_D)$ and $\bar{N} \mapsto \text{cond}(\mathbf{E}_D)$ for $\tau = \tau_1$, $\tau = \tau_2$ and $\tau = \tau_3$ (left to right), comparing in each plot the 3 grids $\mathcal{LL}_N$, $\mathcal{CS}_N$ and $\mathcal{IS}_N$. The grid $\mathcal{LL}_N$ is associated to the larger condition numbers. The grid $\mathcal{IS}_N$ is associated to the smaller ones. The grid $\mathcal{CS}_N$ is intermediate. In each case, $\text{cond}(\mathbf{A}_D) \leq \text{cond}(\tilde{\mathbf{E}}_D)$.

$\mathcal{CS}_{32}$ and $\mathcal{IS}_{25}$. Each grid contains approximately 6200 nodes. Blue symbols correspond to a 0-distance (up to computer accuracy). In each case, a value d such that $\mathcal{Y}_d \subset \mathcal{U}_D$ is indicated by a red line. Similar plots are shown for the following grid parameters: $N \in [\![1;30]\!]$ (for $\mathcal{LL}_N$), $N \in [\![1;32]\!]$ (for $\mathcal{CS}_N$) and $N \in [\![1;25]\!]$ (for $\mathcal{IS}_N$). Calling $d_{\max}$ the maximum degree such that $\mathcal{Y}_d \subset \mathcal{U}_D$, it turns out from Table 2 that $d_{\max}(\mathcal{LL}_N) < d_{\max}(\mathcal{CS}_N) < d_{\max}(\mathcal{IS}_N)$. This means that for a fixed number of nodes $\bar{N}$, the Icosahedral grid correctly represents a larger space $\mathcal{Y}_d$ than the grids $\mathcal{LL}_N$ and $\mathcal{CS}_N$.

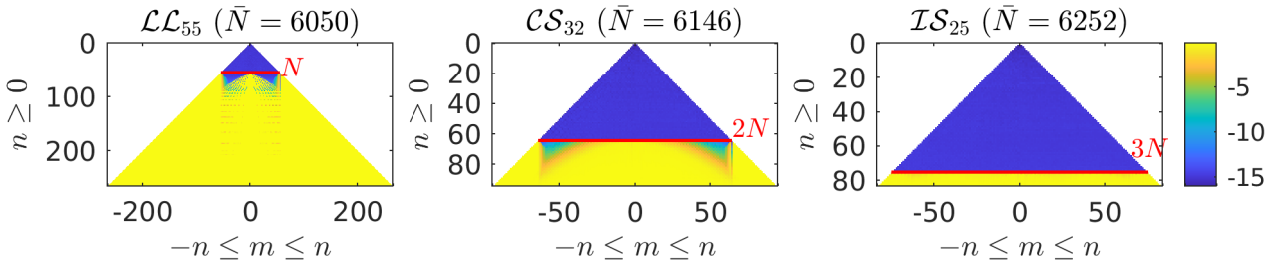

FIGURE 5. Distance $dist(Y_n^*, \mathcal{U}_D)$ in (24) using log scale, for the grids $\mathcal{LL}_{55}$, $\mathcal{CS}_{32}$ and $\mathcal{IS}_{25}$. The better results are obtained for the Icosahedral grid.

Grid	d **such that** $\mathcal{Y}_d \subset \mathcal{U}_D$
$\mathcal{LL}_N$	$N - 1 \approx 0.71\sqrt{\bar{N}}$
$\mathcal{CS}_N$	$2N - 1 \approx 0.82\sqrt{\bar{N}}$
$\mathcal{IS}_N$	$3N - 1 \approx 0.95\sqrt{\bar{N}}$

TABLE 2. Approximate degree d such that $\mathcal{Y}_d \subset \mathcal{U}_D$ for the grids $\mathcal{LL}_N$, $\mathcal{CS}_N$ and $\mathcal{IS}_N$. The function $\bar{N} \mapsto d$ grows at the fastest rate with $\mathcal{IS}_N$ and at the smallest with $\mathcal{LL}_N$. The rate is intermediate with $\mathcal{CS}_N$.

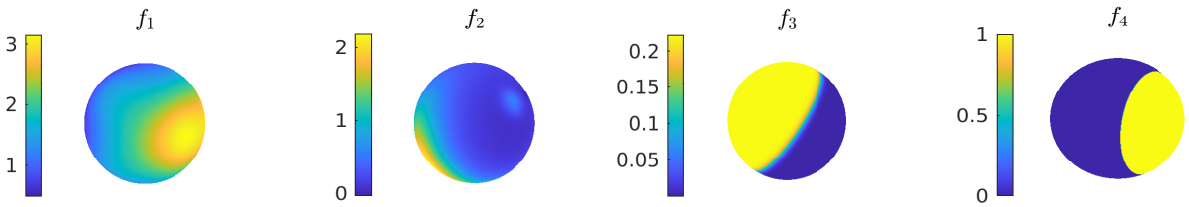

FIGURE 6. Functions f_i $(1 \leq i \leq 4)$. The function f_1, f_2 and f_3 are regular with f_1 polynomial. The function f_4 is discontinuous.

4.3. **Interpolation accuracy.** Here we interpolate the 4 functions f_1, f_2, f_3 and f_4 defined on $\mathbb{S}^2$ with the space $\mathcal{U}_D$ defined in (13). The threshold τ in Sec. 4 is picked as $\tau = \tau_2 = 10^{-2}$.

$$f_1(x,y,z) = 1 + x + y^2 + yx^2 + x^4 + y^5 + x^2y^2z^2 \tag{25}$$

$$\begin{aligned} f_2(x,y,z) = &\tfrac{3}{4}\exp\left(-\tfrac{(9x-2)^2}{4} - \tfrac{(9y-2)^2}{4} - \tfrac{(9z-2)^2}{4}\right) \\ &+ \tfrac{3}{4}\exp\left(-\tfrac{(9x+1)^2}{49} - \tfrac{9y+1}{10} - \tfrac{9z+1}{10}\right) \\ &+ \tfrac{1}{2}\exp\left(-\tfrac{(9x-7)^2}{4} - \tfrac{(9y-3)^2}{4} - \tfrac{(9z-5)^2}{4}\right) \\ &- \tfrac{1}{5}\exp\left(-(9x-4)^2 - (9y-7)^2 - (9z-5)^2\right) \end{aligned} \tag{26}$$

$$f_3(x,y,z) = \frac{1}{9}\left(1 + \tanh(-9x - 9y + 9z)\right) \tag{27}$$

$$f_4(x,y,z) = \frac{1}{2}\left(1 + \operatorname{sign}\left(x - \frac{1}{2}\right)\right) \tag{28}$$

Since $f_1 \in \mathcal{Y}_6 \subset \mathcal{U}_D$, it is expected that $\mathcal{I}_{\bar{N}} f_1 = f_1$ for all grids. The functions f_2 and f_3 are regular but with an infinite SH expansion, thus an error is expected. The function f_4 [5] is discontinuous, with an infinite SH expansion as well. Fig. 6 displays the levels of the functions f_i $(1 \leq i \leq 4)$. Note that the interpolate $\mathcal{I}_{\bar{N}} f_4$ displays oscillations on a fine grid, similar to the "Runge phenomenon". Fig. 7 reports the relative error

$$\bar{N} \mapsto \frac{\|\mathcal{I}_{\bar{N}} f_i - f_i\|_\infty}{\|f_i\|_\infty} \tag{29}$$

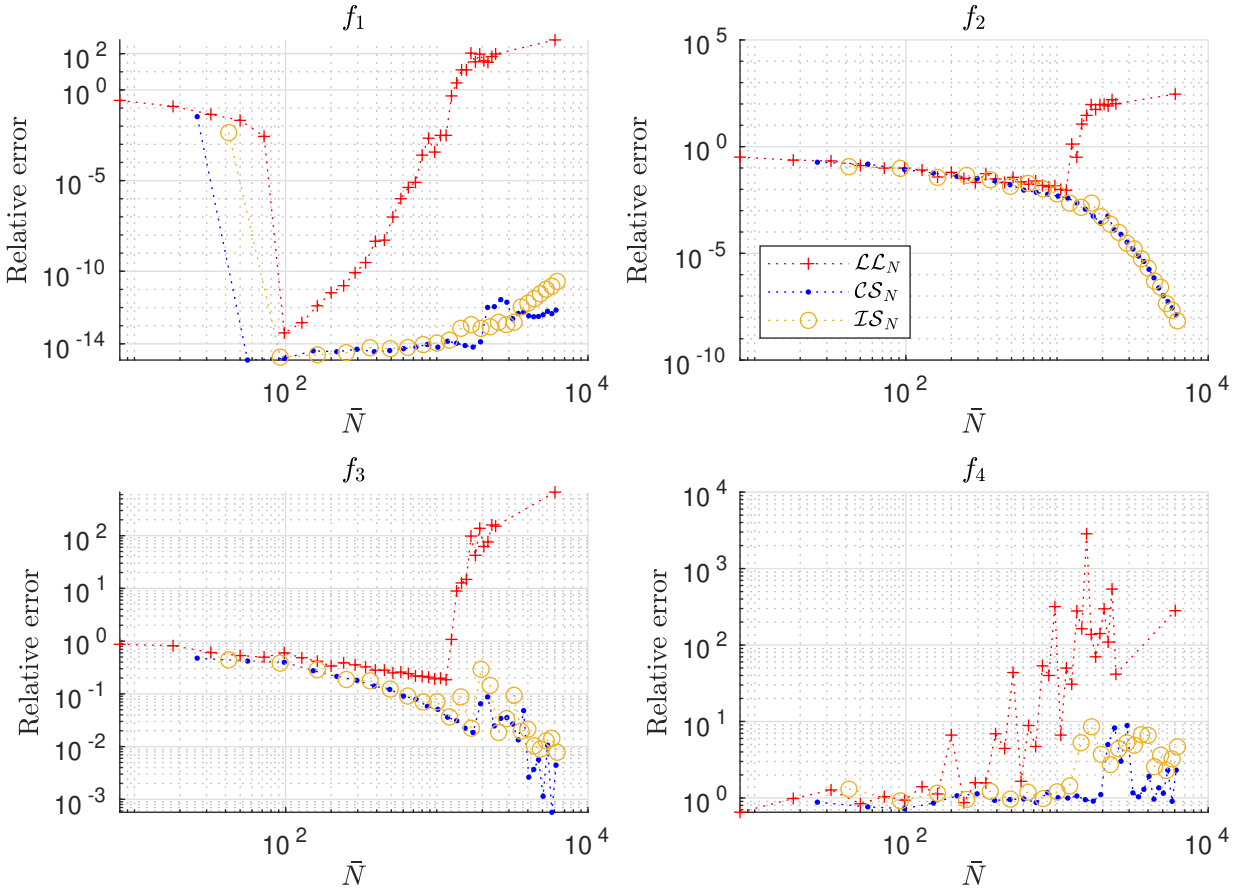

FIGURE 7. Plots of the relative error (29) for the functions f_i, $i = 1, 2, 3, 4$. Convergence is observed for $\bar{N}$ large for the regular functions f_1, f_2 and f_3 for $\mathcal{CS}_N$ and $\mathcal{IS}_N$ but not for $\mathcal{LL}_N$.

with $\|u\|_\infty = \max_{x_j \in \mathcal{LL}_{100}} |u(x_j)|$.

4.4. **Quadrature.** In [5, Theorem 8], a quadrature rule using the nodes of the Cubed-Sphere $\mathcal{CS}_N$ as quadrature nodes has been considered. Here, the same method is extended to the grids $\mathcal{LL}_N$ and $\mathcal{IS}_N$. Let $u : \mathbb{S}^2 \to \mathbb{R}$ be a given function. Define

$$\mathcal{Q}_{\bar{N}} u \triangleq \int_{\mathbb{S}^2} \mathcal{I}_{\bar{N}}[u|_{\mathcal{G}_{\bar{N}}}](x) d\sigma. \tag{30}$$

Since the set of function $(Y_n^m)_{0 \le |m| \le n}$ is an orthonormal basis of $L^2(\mathbb{S}^2)$ we have

$$\int_{\mathbb{S}^2} Y_n^m(x) d\sigma = \langle Y_n^m, Y_0^0 \rangle_{L^2(\mathbb{S}^2)} = \begin{cases} \sqrt{2\pi} & \text{if } m = n = 0 \\ 0 & \text{else.} \end{cases} \tag{31}$$

For this reason $\mathcal{Q}_{\bar{N}} u$ is proportional to the first coefficient of the SH decomposition and

$$\mathcal{Q}_{\bar{N}} u = \sum_{j=1}^{\bar{N}} \omega_j u(x_j) \tag{32}$$

with $[\omega_j]_{1 \le j \le \bar{N}} = (\tilde{\mathbf{V}}_D \tilde{\mathbf{E}}_D^{-\intercal} \mathbf{U}_D^\intercal) \begin{bmatrix} \sqrt{4\pi} & 0 & \cdots & 0 \end{bmatrix}^\intercal$. Here again, the threshold τ is selected as $\tau = \tau_2 = 10^{-2}$. With this choice, the weights $[\omega_j]_{1 \le j \le \bar{N}}$ have been observed positive for $\mathcal{CS}_N$ $(1 \le N \le 32)$ and $\mathcal{IS}_N$ $(1 \le N \le 25)$. (There is no proof of this statement at the moment). However, with $\mathcal{LL}_N$ $(N \ge 25)$, some weights are observed negatives.

The quadrature formula $\mathcal{Q}_{\bar{N}}$ is tested against the series of functions in Table 3. In Fig. 8, we report the worst relative error $\varepsilon(f_i)$ among 1000 random rotations of the grid. For a given function f_i, the relative error

Function f_i	$\int_{\mathbb{S}^2} f_i(x)d\sigma$	**References**
f_1	$216\pi/15$	[3]
f_2	$6.6961822200736179523\cdots$	[1, 9]
f_3	$4\pi/9$	[3]
f_4	π	[5]

TABLE 3. Exact mean value for the 4 functions f_i, $i = 1, 2, 3, 4$.

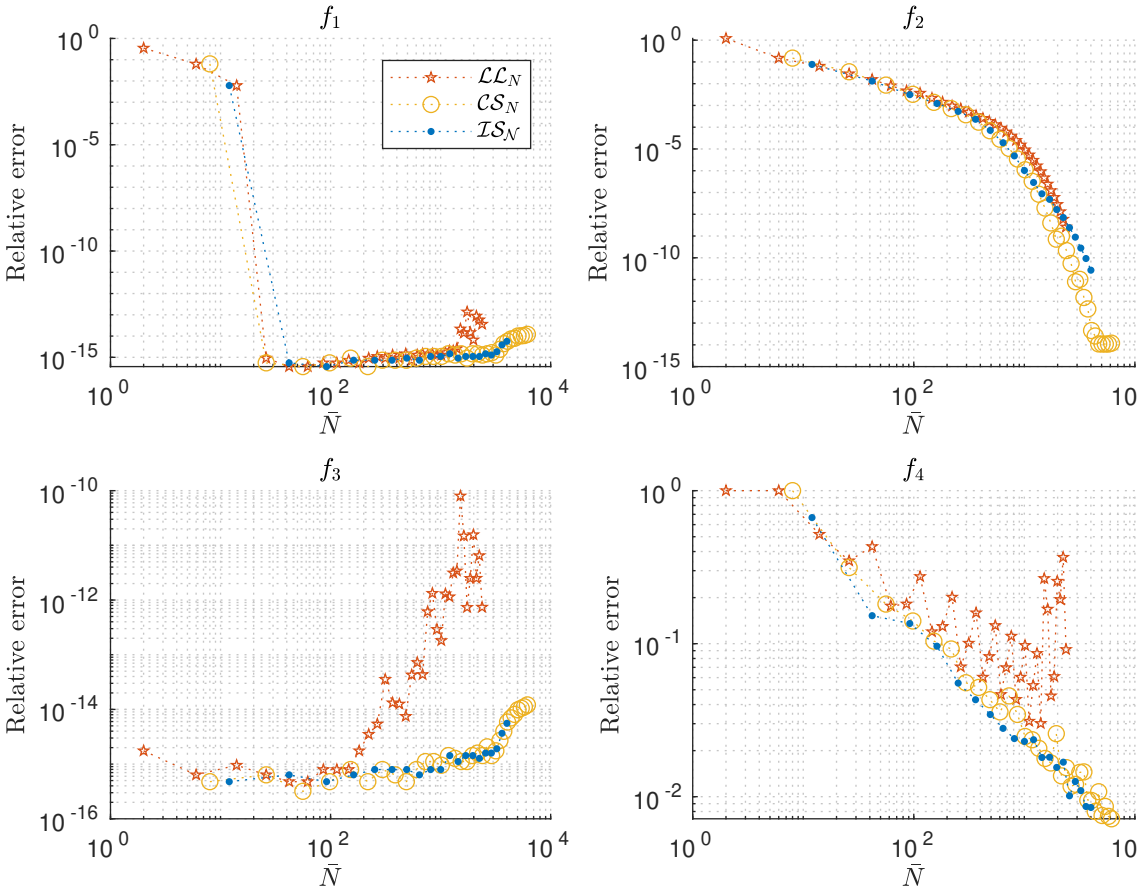

FIGURE 8. Plots of the relative quadrature errors (31) for the 3 grids $\mathcal{LL}_N$, $\mathcal{CS}_N$ and $\mathcal{IS}_N$ in function of the number of nodes $\bar{N}$ for the functions f_i, $i = 1, 2, 3, 4$. The worst error is retained among 1000 random orthogonal transformations of the grid. For each grid, the quadrature rules converge to the exact value when $\bar{N}$ increases. The grids $\mathcal{CS}_N$ and $\mathcal{IS}_N$ give the best results.

is given by

$$\varepsilon(f_i) : \bar{N} \mapsto \frac{\left| \mathcal{Q}_{\bar{N}} f_i - \int f_i(x)d\sigma \right|}{\left| \int f_i(x)d\sigma \right|}.$$

The fact that $f_1 \in \mathcal{Y}_6$ is a polynomial function implies an exact quadrature is exact assuming a large enough number of grid nodes and a suitable condition number. Moreover, since the function f_2 is regular, the convergence is obtained for all quadrature rules. The function f_3 is smooth but divides the sphere in two with a sharp interface. However, all the quadrature rules provide accurate results. Instabilities are visible on the finest grids, particularly for the grid $\mathcal{LL}_{\bar{N}}$. This can be related to the condition number $\text{cond}(\tilde{\mathbf{E}}_D)$. Even so, the error level is $< 10^{-10}$. The function f_4 is not regular. For this reason, it is certainly the most difficult to integrate on the sphere. The quadrature rules we have developed for $\mathcal{CS}_{\bar{N}}$ and $\mathcal{IS}_{\bar{N}}$ give results similar to those of Lebedev's formula. Unfortunately, the weights related to the grid $\mathcal{LL}_{\bar{N}}$ do not give good results and seem to suffer from numerical instabilities on the finest grids. By analysing the weights, it appears some

values $(\omega_j)_{1\leq j\leq \bar{N}}$ are negative and with a large amplitude close to the poles. Once again, this behaviour can be related to $\mathrm{cond}(\tilde{\mathbf{E}}_D)$.

5. Summary

We have considered interpolation and quadrature based on data located on a spherical grid $\mathcal{G}_{\bar{N}} \subset \mathbb{S}^2$. A specific subspace of SH fuctions associated to the grid by the algorithm 1 is introduced for that purpose. Our numerical computations are based on the special echelon factorization of the associated Vandermonde matrix. This factorization is implemented with an incremental algorithm already devised in [4–6] in the case of the Cubed Sphere. The procedure depends on the thresholding parameter τ in Sec. , which determines the effective value of the matrix rank at each step. Selecting this threshold value τ therefore plays a crucial role. A series of numerical experiments have been presented on the three grids Lon/Lat, Cubed-Sphere and Icosahedral. The effect of the parameter τ is analyzed as well as the shape of the interpolation SH functions space $\mathcal{U}_D$. The grid $\mathcal{CS}_N$ and $\mathcal{IS}_N$ give comparable results, both superior to the ones obtained with the grid $\mathcal{LL}_N$. This does not discard the interest of the Lon/Lat grid. It simply means that our interpolation procedure is not adapated to the grid $\mathcal{LL}_N$.

Acknowledgments

This work was supported by the French National program LEFE (Les Enveloppes Fluides et l'Environnement).

References

[1] C. An and S. Chen. Numerical integration over the unit sphere by using spherical t-design. *arXiv:1611.02785v1*, 2016.
[2] K. Atkinson and W. Han. *Spherical harmonics and approximations on the unit sphere: an introduction*, volume 2044. Springer Science & Business Media, 2012.
[3] C. H. Beentjes. Quadrature on a spherical surface. *Technical report, Oxford University - https://cbeentjes.github.io/notes/2015-Quadrature-Sphere*, 2015.
[4] J.-B. Bellet. Mathematical and numerical methods for three-dimensional reflective tomography and for approximation on the sphere. Habilitation thesis, Université de Lorraine, 2023.
[5] J.-B. Bellet, M. Brachet, and J.-P. Croisille. Quadrature and symmetry on the Cubed Sphere. *Journal of Computational and Applied Mathematics*, 409:114142, 2022.
[6] J.-B. Bellet, M. Brachet, and J.-P. Croisille. Interpolation on the cubed sphere with spherical harmonics. *Numerische Mathematik*, 153(2):249–278, 2023.
[7] F. Dai and Y. Xu. Moduli of smoothness and approximation on the unit sphere and the unit ball. *Advances in Mathematics*, 224(4):1233–1310, 2010.
[8] S. Kunis, H. M. Möller, and U. von der Ohe. Prony's method on the sphere. *The SMAI Journal of Computational Mathematics*, 5:87–97, 2019.
[9] B. Portelenelle and J.-P. Croisille. An efficient quadrature rule on the cubed sphere. *Journal of Computational and Applied Mathematics*, 328:59–74, 2018.
[10] C. Ronchi, R. Iacono, and P. S. Paolucci. The "cubed sphere": a new method for the solution of partial differential equations in spherical geometry. *Journal of Computational Physics*, 124(1):93–114, 1996.
[11] R. Sadourny, A. Arakawa, and Y. Mintz. Integration of the nondivergent barotropic vorticity equation with an icosahedral-hexagonal grid for the sphere. *Monthly Weather Review*, 96(6):351–356, 1968.
[12] N. Wang and J.-L. Lee. Geometric properties of the icosahedral-hexagonal grid on the two-sphere. *SIAM Journal on Scientific Computing*, 33(5):2536–2559, 2011.

† Université de Poitiers, CNRS, LMA, F-86000 Poitiers, France
Email address: jean-baptiste.bellet@math.univ-poitiers.fr, matthieu.brachet@math.univ-poitiers.fr

‡ Université de Lorraine, CNRS, IECL, F-57000 Metz, France
Email address: jean-pierre.croisille@univ-lorraine.fr